Bioinspired Simultaneous Changes in Fluorescence Color, Brightness and Shape of Hydrogels Enabled by AIEgens

Zhao Li[1,2], Xiaofan Ji[1,2], Junyi Gong[1,2], Yubing Hu[1,2], Wenjie Wu[1,2], Xinnan Wang[1,2], Hui-Qing Peng[1,2], Ryan T. K. Kwok[1,2], Jacky W. Y. Lam[1,2,*] and Ben Zhong Tang[1,2,3,*]

[1]Department of Chemistry, Hong Kong Branch of Chinese National Engineering Research Center for Tissue Restoration and Reconstruction and Institute for Advanced Study, The Hong Kong University of Science and Technology, Clear Water Bay, Kowloon, Hong Kong, China.

[2]HKUST-Shenzhen Research Institute, No. 9 Yuexing 1st RD, South Area, Hi-tech Park, Nanshan, Shenzhen 518055, China.

[3]Center for Aggregation-Induced Emission, SCUT-HKUST Joint Research Institutes, State Key Laboratory of Luminescent Materials and Devices, South China University of Technology, Guangzhou, 510640, China.

KEYWORDS: simultaneous, changes, fluorescence color, fluorescence brightness, complex shape, stimuli-responsive, aggregation-induced emission luminogens (AIEgens), bilayer hydrogel actuators.

ABSTRACT: Development of stimuli-responsive materials with complex practical functions is significant for achieving bioinspired artificial intelligence. It is challenging to fabricate stimuli-responsive hydrogels showing simultaneous changes in fluorescence color, brightness and shape in response to one stimulus. Herein a bilayer hydrogel strategy was designed by utilizing an aggregation-induced emission luminogen (AIEgen) tetra-(4-pyridylphenyl)ethylene (TPE-4Py) to fabricate hydrogels with the above capabilities. Bilayer hydrogel actuators with ionomer of poly(acrylamide-r-sodium 4-styrenesulfonate) (PAS) as matrix of both active and passive layers and TPE-4Py as the core function element in the active layer were prepared. At acidic pH, the protonation of TPE-4Py led to fluorescence color and brightness changes of the actuators and the electrostatic interactions between the protonated TPE-4Py and benzenesulfonate groups of PAS chains in the active layer caused the actuators to deform. The proposed TPE-4Py/PAS-based bilayer hydrogel actuators with such responsiveness to stimulus provide pregnant insights in the design of intelligent systems and are highly attractive material candidates in fields of 3D/4D printing, soft robots and smart wearable devices.

INTRODUCTION

In nature, numerous biological systems are intelligent.[1,2] Many species are able to simultaneously change their colors and shapes in response to stimulus. For an example, chameleons can rapidly alter their skin color when they move into a new place to blend into its different surrounding environment.[3] Mimic octopuses, on the other hand, are able to change both their color and shape in order to camouflage or hunt.[4,5] Frilled-necked lizards spread out their frills and the frills simultaneously turn to bright yellow, orange or red when they are frightened or during courtship.[6,7] Besides animals, some plants show also the ability to simultaneously change their colors and shapes. *Brunfelsia acuminata* also known as "Yesterday-Today-Tomorrow" of which flowers open purple, fade to lavender and finally to white during blooming process is a typical example.[8,9] *Quisqualis indica*, on the other hand, has white and horizontally oriented flowers that open at dusk and change to pink and later to red on the following day. The flowers become pendulous by simultaneously changing their orientation during their florescence.[10,11] *Tibouchina pulchra* flora color changes from white in the first day to pink in the following days of anthesis.[12] Such a process of simultaneous color and shape changes of the flowers is interpreted as a warning mechanism for pollinators to avoid old flowers.[13]

Scientific researchers are pursuing to fabricate free-standing intelligent artificial materials. One promising approach is to use stimuli-responsive materials.[14,15] Because of this, they have been capturing much interest.[16-18] Among them, smart hydrogel[19-22] is an important member and can change its volume or other properties dramatically under stimuli such as temperature,[23-25] pH,[26,27] irradiation,[28,29] electric field,[30] magnetic field,[31] ionic strength,[32] a specific chemical[33,34] and so on. Inspired by the biological behaviors, a number of attempts have been reported to construct stimuli-responsive hydrogels with capacities of undergoing shape deformation[21,35-43] in the presence of stimulus utilizing the bilayer technique[44] or color change

including fluorescence change.[45-48] However, most of the hydrogels show either of shape change or color change. Although there are very few reports on deformable hydrogels showing stimulus-induced fluorescence color change, the shape change and the fluorescence change are independent. The two changes are based on different elements in the hydrogel or are triggered by different stimuli. It is thus challenging to realize response hydrogels with simultaneous changes of fluorescence color, brightness and shape based on one stimulus.

It is critical to select a suitable fluorophore as the sole source of the changes to realize the above goal. Aggregation-induced emission luminogens (AIEgens)[49] are non-emissive as isolated species in good solvents but are highly emissive in poor solvents as aggregates.[50] Such an aggregation-induced emission (AIE) phenomenon is believed to be caused by the restriction of intramolecular motion (RIM) in the aggregated state.[51] The strong emission of AIEgens in the aggregated, solid or restricted states makes them suitable to be applied in semi-solid hydrogel systems.[52,53] As a burgeoning scientific research field, AIE has attracted intense interest and has been applied in numerous areas.[54-57] The fast and wide development of AIEgens is due to their superiorities of comprehensible mechanism, accessible designability, easy functionalization, large absorptivity, high brightness in the restricted state and low background noise. Until now, a large variety of stimuli-responsive AIEgens have been developed and applied,[58-63] and many of them experience fluorescence color or brightness changes when they are ionized[64-69] and are potential building blocks for the construction of supramolecular materials.[70,71] Therefore, AIEgens are ideal candidates in the design and fabrication of stimuli-responsive hydrogel systems fluorescence color, brightness and shape changes in response to stimulus.

In this study, we reported the design and construction of bioinspired hydrogels with abilities of simultaneous fluorescence color and intensity changes as well as complex shape deformation by utilizing AIEgens and the bilayer hydrogel technique.[44] The pH-responsive AIEgen called tetra-(4-pyridylphenyl)ethylene (TPE-4Py) was used to impart the formed bilayer hydrogel actuators with the above changes and an ionomer namely poly(acrylamide-*r*-sodium 4-styrenesulfonate (PAS) was used as the matrix of the actuators. When the actuators were immersed in acidic aqueous solution, they could change their fluorescence color, brightness and actuator shape simultaneously. The ability for shape change was achieved by asymmetrical distribution of TPE-4Py aggregates in the two layers of the actuators. At low pH, the protonation of TPE-4Py embedded in the active layer of the actuators caused altered fluorescence color and intensity. Meanwhile, electrostatic interactions between the protonated TPE-4Py and the benzenesulfonate groups of PAS chains led to the shape deformation of the actuators. The resulting TPE-4Py/PAS-based bilayer hydrogel actuators with simultaneous stimulus-induced fluorescence color, brightness and complex shape changes provide new insights in the design of advanced bioinspired intelligent systems with complex practical functions and may have potential applications in fields of 3D/4D printing, soft robots and smart drug delivery systems.

RESULTS AND DISCUSSION

Design of Bilayer Hydrogel Actuators with Simultaneous Fluorescence Color, Brightness and Complex Shape Changing Property. It is a key that the fluorescence color changing function, the fluorescence brightness changing function and the complex shape deformation function are built based on one element in the hydrogel actuator to realize its ability of simultaneous fluorescence color, brightness and complex shape changing. AIEgen is a good candidate of the element. TPE-4Py, a classical AIEgen with pH-responsiveness was selected.[72-74] It can form aggregates in water with neutral pH to form a suspension due to its hydrophobicity. The aggregates emit strong sapphire fluorescent light based on the effect of the restriction of intramoelcular rotation (RIR).[75,76] When the pH value of the suspension is decreased, TPE-4Py is able to protonates to form the tetra-protonated TPE-4Py (4H-TPE-4Py^{4+}) and the fluorescence color red shifts due to the enhanced intramolecular charge transfer (ICT) process.[77,78] In addition, the protonation of TPE-4Py increases the solubility of it largely, which reduces the fluorescence brightness obviously due to the enhancement of intramoelcular rotation (EIR) effect. Taking advantage of the protonation process of TPE-4Py during the pH decreasing process, an ionomer PAS that carries negatively charged groups was used as the matrix of the actuator. The PAS hydrogel was fabricated through *in situ* random copolymerization of monomers acrylamide (AAm) and sodium 4-styrenesulfonate (NaSS) and a cross-linker *N,N'*-methylenebisacrylamide (BIS). TPE-4Py/PAS-based bilayer hydrogel actuators with TPE-4Py as the functional element and PAS hydrogel as the matrix were designed, in which a PAS hydrogel layer acted as the passive layer and a TPE-4Py aggregates encapsulated PAS hydrogel layer acted as the active layer (Figure 1a). In the neutral medium, the TPE-4Py aggregates were physically encapsulated in the PAS hydrogel in the active layer and didn't have interactions with network chains of the hydrogel. When the bent bilayer hydrogel actuator was immersed in an acidic aqueous solution, TPE-4Py in the aggregates protonated and dissolved gradually, and electrostatic interactions were occurred between protonated pyridyl groups in the formed 4H-TPE-4Py^{4+} and benzenesulfonate groups on hydrogel network chains in the active layer (Figure 1b). The 4H-TPE-4Py^{4+} acted as the additional physical cross-linking point and caused the active layer to shrink, and the hydrogel actuator gradually unbent.[79] Meanwhile, the fluorescence color of the hydrogel actuator red shifted gradually due to the protonation of TPE-4Py. Because the dissolved 4H-TPE-4Py^{4+} formed electrostatic interactions with network ionomer chains, the intramolecular rotation of 4H-TPE-4Py^{4+} were restricted. Thus, the brightness of the red shifted fluorescent light enhanced and visualized.

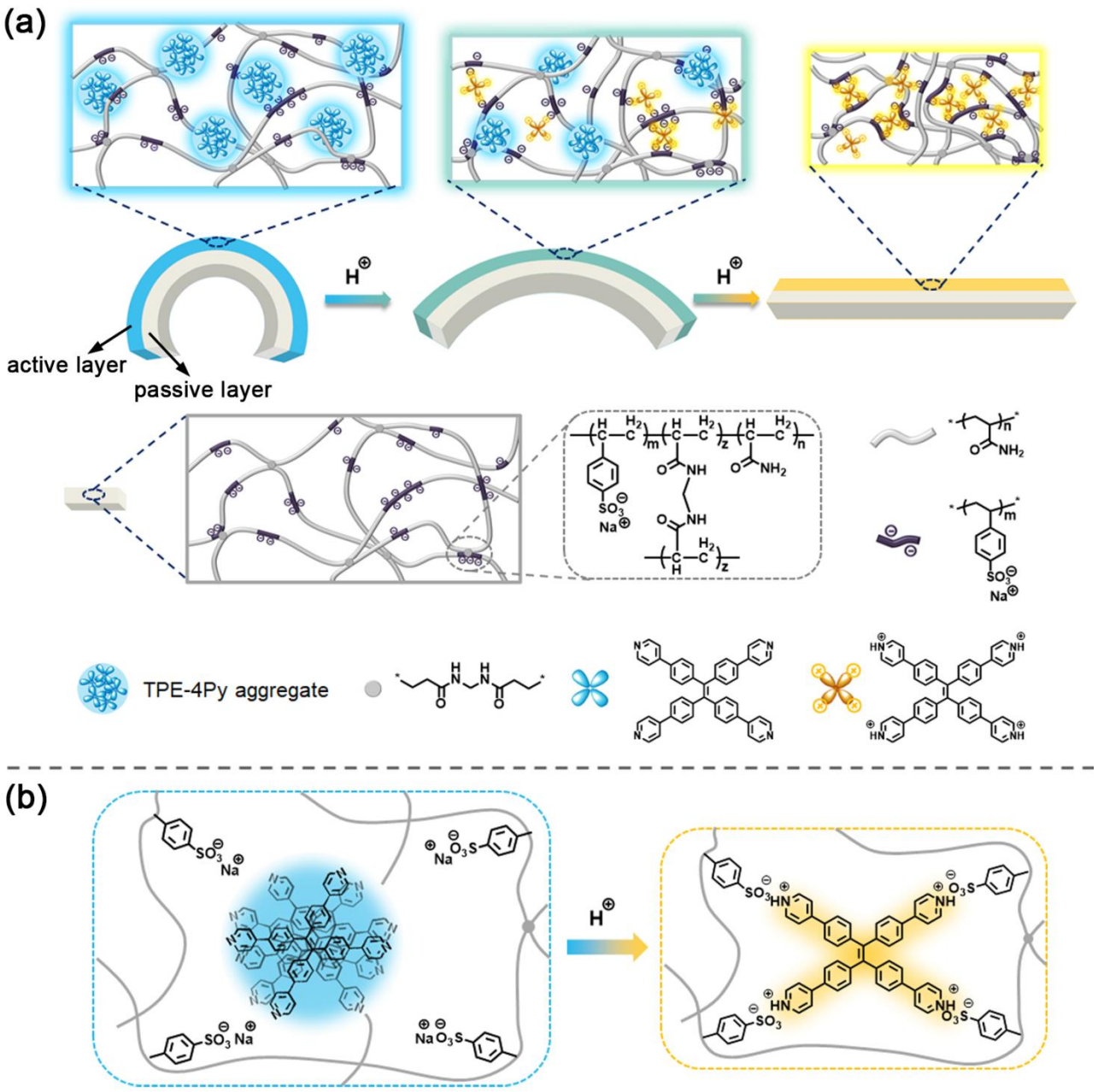

Figure 1. (a) Schematic illustration of simultaneous changes in fluorescent color and brightness and 3D shape of a TPE-4Py/PAS-based bilayer hydrogel actuator and the mechanism involved. (b) When the medium of the hydrogel actuator becomes acidic, the TPE-4Py in an aggregate is protonated and dissolves, and electrostatically interacts with benzenesulfonate groups on network chains in the active layer.

The pH-Responsiveness of TPE-4Py. As the core function element in bilayer hydrogel actuators in the present work, TPE-4Py was first investigated. A series of TPE-4Py aqueous suspensions with different pH values from 2.09 to 10.13 were prepared using pH buffers. Figure 2a shows their photographs under 365-nm UV illumination. Their PL spectra were measured (Figure 2b) and the pH dependences of the wavelength at the maximum PL intensity (λ_{max}) and the maximum PL intensity (I_{max}/I_0) were depicted in Figure 2c. It can be seen from Figure 2c that λ_{max} has little change and I_{max}/I_0 increases slightly with pH increasing from 6.98 to 10.13. When the pH value decreases from 6.98 to 2.09, λ_{max} first decreases slightly, then increases, followed by a sharp decline and a sharp large increment, and reaches the equilibrium of about 536 nm with pH value below 2.96. Meanwhile, with the pH value decreasing from 6.98 to 2.09, I_{max}/I_0 first decreases slightly, then increases, followed by a sharp large decrease, and reaches the equilibrium with pH value below 3.58. In neutral medium, TPE-4Py forms aggregates in amorphous state (Figure S7, S8 and S9) in the aqueous buffer solution. The restriction of intramolecular rotation of TPE-4Py leads to the strong sapphire emission. When the pH value gradually decreases into the faintly acidic range, the solu-

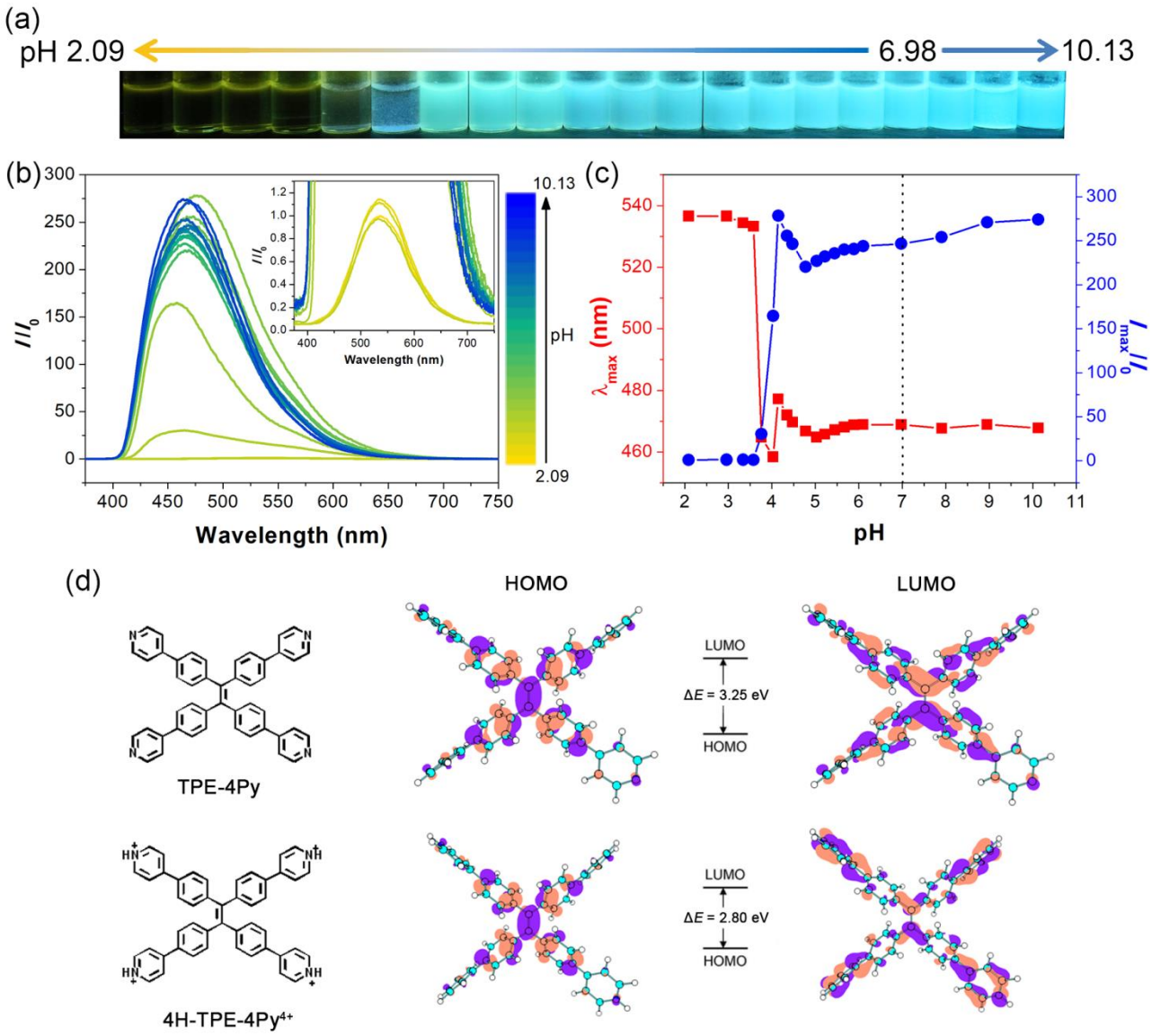

Figure 2. (a) Photographs of TPE-4Py aqueous suspensions (c = 10^{-4} M) with different pH values. (pH values of the suspensions from left to right are 2.09, 2.96, 3.34, 3.58, 3.76, 4.03, 4.15, 4.35, 4.48, 4.78, 5.03, 5.22, 5.45, 5.67, 5.89, 6.10, 6.98, 7.91, 8.95 and 10.13 respectively.) (The photographs were taken under 365-nm UV illumination.) (b) PL spectra of the suspensions in (a). Insets are amplified PL spectra with Y axis being magnified with 230 times. (I is the PL intensity of the suspensions with different pH values and I_0 is the maximum PL intensity of the suspension with pH of 2.09.) (λ_{ex} = 365 nm) (c) Wavelength at the maximum PL intensity (λ_{max}) and the maximum PL intensity (I_{max}/I_0) of the suspensions as a function of pH. (I_{max} is the maximum PL intensity of the suspensions with different pH values.) (d) Molecular structures and molecular orbital amplitude plots of HOMO and LUMO energy levels of TPE-4Py and 4H-TPE-4Py^{4+}.

bility of TPE-4Py increases gradually and the fluorescent intensity of the suspension decreases slightly due to the EIR effect. When the pH value continues to decrease below 5 (from 4.78 to 4.15), TPE-4Py gradually protonates. The emerging obvious intramolecular charge transfter (ICT) process causes the fluorescent emission to red shifts. Meanwhile, because the solubility of TPE-4Py further increases, nano-crystals of it form which was demonstrated by scanning electron microscope (SEM) and polarizing optical microscope (POM) (Figure S8 and S9). Crystallization-enhanced emission (CEE) effect[59] leads to the increment of the fluorescent intensity of the suspension. With the pH value continuing to decrease to 3.76, further increase of the solubility leads to the formation of TPE-4Py crystal (Figure S7, S8 and S9) which rendering the blue shifted fluorescent emission.[80,81] The CEE effect is supposed to lead to fluorescent intensity increase. However, a mass of TPE-4Py molecules protonate and dissolve in this pH medium. The EIR effect causes their emission pretty weak. Thus the suspension shows reduced intensity and blue shifted emission. When the pH value further decreases below 3.7, all TPE-4Py molecules protonate to 4H-TPE-4Py^{4+} with yellow emission. The dissolution of the 4H-TPE-4Py^{4+} activates its intramolecular rotation, leading to a very weak fluorescent intensity.

DFT calculation was used to simulate the molecular orbital amplitudes of HOMO and LUMO energy levels of TPE-4Py and 4H-TPE-4Py^{4+} (Figure 2d). Based on the calculated energy gaps (ΔE) between HOMO and LUMO energy levels, UV-Vis absorption spectra of TPE-4Py and 4H-TPE-4Py^{4+} were predicted in Figure S10a. UV-Vis spectra of TPE-4Py in $CHCl_3$ and TFA/$CHCl_3$ mixture (1/9, V/V) were measured (Figure S10b). The spectrum of TPE-4Py in the TFA/$CHCl_3$ mixed solvent is consistent with that of predicted 4H-TPE-4Py^{4+}. In addition, ^{1}H NMR spectrum in Figure 3e (II) of the D_2O solution of TPE-4Py with pH value of 2.0 also demonstrates TPE-4Py transforms into 4H-TPE-4Py^{4+} at this pH value. Thus, in the TFA/$CHCl_3$ mixed solvent, TPE-4Py protonates into 4H-TPE-4Py^{4+}. UV-Vis absorption spectra of TPE-4Py aqueous suspensions with pH values from 2.09 to 4.03 were also measured (Figure S10c) and they are all consistent with the spectrum of 4H-TPE-4Py^{4+}. Therefore, TPE-4Py protonates to form 4H-TPE-4Py^{4+} with pH value below 4.

The pH-Responsive Fluorescence Color, Brightness and Volume Changing Properties of TPE-4Py/PAS-Based Monolayer Hydrogels. After the pH-responsiveness of TPE-4Py in its aqueous suspension was made clear, monolayer hydrogels based on the TPE-4Py aggregate and the PAS hydrogel were constructed. **M1** to **M5** monolayer hydrogel film (thickness: 1 mm) samples with increased TPE-4Py concentration were prepared according to recipes in Table S1. PAS hydrogel **M0** without TPE-4Py was also prepared as the blank sample for the comparison. The hydrogel films were swollen in DI water to the equilibrium before further experiments.

Rectangular hydrogel sheets of **M0** to **M5** with the size of about 10 mm × 10 mm were immersed in aqueous solutions with pH values from 7.30 to 1.85 for 17 h. Photographs of the samples under day-light and 365-nm UV illumination were shown in Figure 3a and Figure S11. Fluorescent emission spectra (Figure S12) of the samples were measured and pH dependences of the λ_{max} and the maximum PL intensity (I_{max}) were depicted in Figure 3b and c. From the photographs and the figures, it can be seen that with the decrease of the pH value, the fluorescent emissions of **M1** to **M5** red shift and the fluorescent intensities of them decrease gradually. Because the blank sample **M0** dose not have fluorescent emission (Figure 3c), the origin of the fluorescent emission of the monolayer hydrogels is TPE-4Py. When the pH value decreases, TPE-4Py in the aggregate in the monolayer hydrogel sample gradually protonates, which leads to the red-shift of the hydrogel sample. Meanwhile, the increase of the solubility of protonated TPE-4Py causes the decrease of its fluorescent intensity due to the EIR effect though the electrostatic interaction between formed pyridyl groups and benzenesulfonate groups on PAS chains restricts the intramolecular rotation of the protonated TPE-4Py to some extent. It can also be seen from the Figure 3c that with the increase of the TPE-4Py concentration from **M1** to **M5**, the fluorescent intensity of the hydrogel sample at a specific pH value increases. This phenomenon can be easily understood that with the increase of the TPE-4Py concentration, the amount of fluorophores increases.

It can also be seen from Figure 3a that with the decrease of the pH value, volumes of the monolayer hydrogel samples of **M1** to **M5** decrease. Masses of **M0** to **M5** before (m_0) and after (m_e) immersing were measured and the shrinkage ratios (η) of them were calculated by the following equation:

$$\eta = \frac{m_0 - m_e}{m_0} \times 100 \quad (1)$$

pH dependences of η of **M0** to **M5** were depicted in Figure 3d. With the decrease of the pH value, hydrogels **M0** to **M5** shrink. η of **M0** slightly increases with pH value decreasing from 7.30 to 3.00. When the pH value further decreases, η of **M0** increases largely up to 59.72%. This may be caused by the ion-shield effect at low pH medium. With the introduction of TPE-4Py aggregates, η of the hydrogel sheets increases compared with that of **M0** in acidic medium. This is caused by the emerged electrostatic interactions between protonated TPE-4Py and benzenesulfonate groups on the hydrogel network chains. In acidic medium, protonated TPE-4Py acts as additional physical cross-linking point. The increase of the cross-linking density causes the hydrogel to shrink. With the increase of the TPE-4Py concentration, η increases from **M1** to **M5** at a specific pH value. This can be easily understood that the higher the TPE-4Py concentration is, the more amount of physical cross-linking points generate in acidic medium.

NMR spectroscopy was used to demonstrate the existence of the electrostatic interaction between protonated TPE-4Py and benzenesulfonate groups on the hydrogel network chains. A linear random copolymer PAAm-*r*-PSS was synthesized (see Supporting Information) as the modal of the hydrogel network chain. A D_2O solution of PAAm-*r*-PSS, a D_2O solution of TPE-4Py and a D_2O solution containing both PAAm-*r*-PSS and TPE-4Py with the pH value of 2.0 were prepared. A D_2O solution containing both PAAm-*r*-PSS and TPE-4Py with the pH value of 7.0 was also prepared. ^{1}H NMR spectra of the solutions were taken and shown in Figure 3e. From the ^{1}H NMR spectrum of the PAAm-*r*-PSS solution (Figure 3e (I)), it can be seen that signals of protons H_a and H_b on the benzenesulfonate group on PAAm-*r*-PSS are located at 7.72 and 7.33 ppm. The shapes and chemical shifts of proton signals on PAAm-*r*-PSS in Figure 3e (I) are identical with that on PAAm-*r*-PSS in D_2O with the pH value of 7.0 in Figure S3. There are four doublet peaks at 8.73, 8.26, 7.80 and 7.48 in the ^{1}H NMR spectrum of TPE-4Py solution in Figure 3e (II), which are assigned to protons H_1, H_2, H_3 and H_4 respectively on 4H-TPE-4Py^{4+}. When PAAm-*r*-PSS and TPE-4Py were mixed in D_2O in neutral medium, the ^{1}H NMR spectrum of the mixture in Figure 3e (III) only contains signals of PAAm-*r*-PSS protons. TPE-4Py in the aggregation state dose not have any proton signals. The spectrum in Figure 3e (III) is identical with the spectrum in Figure 3e (I). This indicates that PAAm-*r*-PSS and TPE-4Py aggregate do not have interactions. When the pH

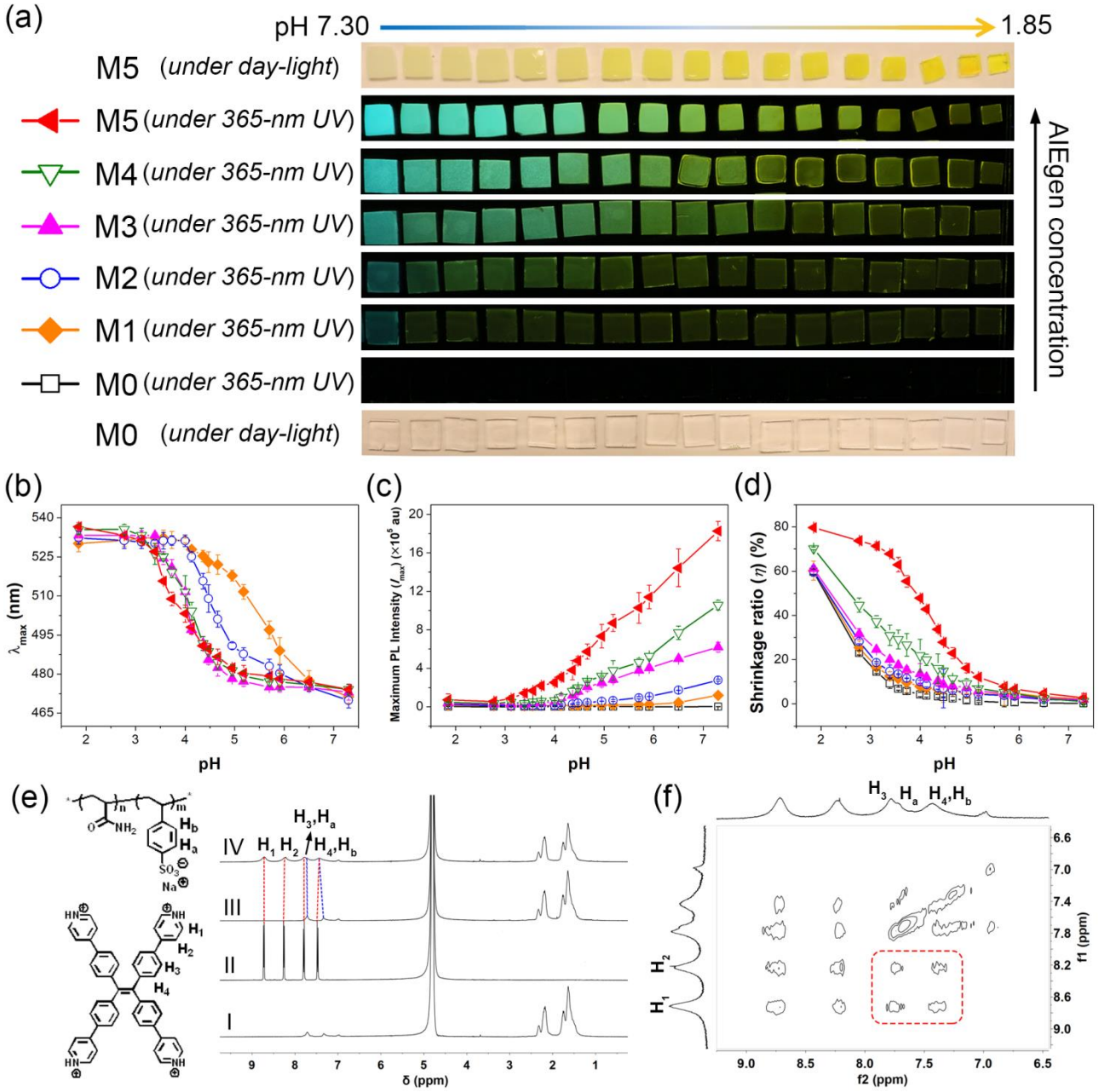

Figure 3. (a) Photographs of monolayer hydrogel samples **Mo** to **M5** after immersed in aqueous solutions with different pH values for 17 h under 365-nm UV illumination. (The pH values of every hydrogel samples from left to right are 1.85, 2.77, 3.12, 3.39, 3.56, 3.73, 4.00, 4.13, 4.36, 4.47, 4.66, 4.95, 5.18, 5.70, 5.91, 6.50 and 7.30 respectively.) (b) λ_{max} of monolayer hydrogel samples as a function of pH after immersed in aqueous solutions with different pH values for 17 h. (c) Maximum PL intensity (I_{max}) of the monolayer hydrogel samples as a function of pH. (d) Shrinkage ratio (η) of the monolayer hydrogel samples as a function of pH. (e) Molecular structures of copolymer network chain of monolayer hydrogel and 4H-TPE-4Py^{4+}, and ^{1}H NMR spectra of (I) a solution of model copolymer PAAm-*r*-PSS (6.00×10^{-3} mM) with pH of 2.0, (II) a solution of TPE-4Py (1.28 mM) with pH of 2.0, (III) a solution of PAAm-*r*-PSS (6.00×10^{-3} mM) and TPE-4Py (1.28 mM) with pH of 7.0, and (IV) a solution of PAAm-*r*-PSS (6.00×10^{-3} mM) and TPE-4Py (1.28 mM) with pH of 2.0. (f) Partial 2D NOESY NMR spectrum of the solution of PAAm-*r*-PSS (6.00×10^{-3} mM) and TPE-4Py (1.28 mM) with pH of 2.0.

value of the mixture was decreased to 2.0, TPE-4Py protonated into 4H-TPE-4Py^{4+} and dissolved, and proton signals of 4H-TPE-4Py^{4+} appeared in the ^{1}H NMR spectrum in Figure 3e (IV). However, the shapes and the chemical shifts of the signals change compared with that in Figure 3e (II). The peaks of protons on 4H-TPE-4Py^{4+} broaden largely and upfield shift when PAAm-*r*-PSS was added. The broadness is related to the dynamics of phenyl and protonated pyridyl groups on 4H-TPE-4Py^{4+}. When 4H-TPE-4Py^{4+} forms electrostatic interactions with PAAm-*r*-PSS, the movements of the phenyl and protonated pyridyl groups on 4H-TPE-4Py^{4+} are restricted and the rotation of the groups reduces.[82] Thus, the proton signals become broad. Besides, the interaction with the benzene-

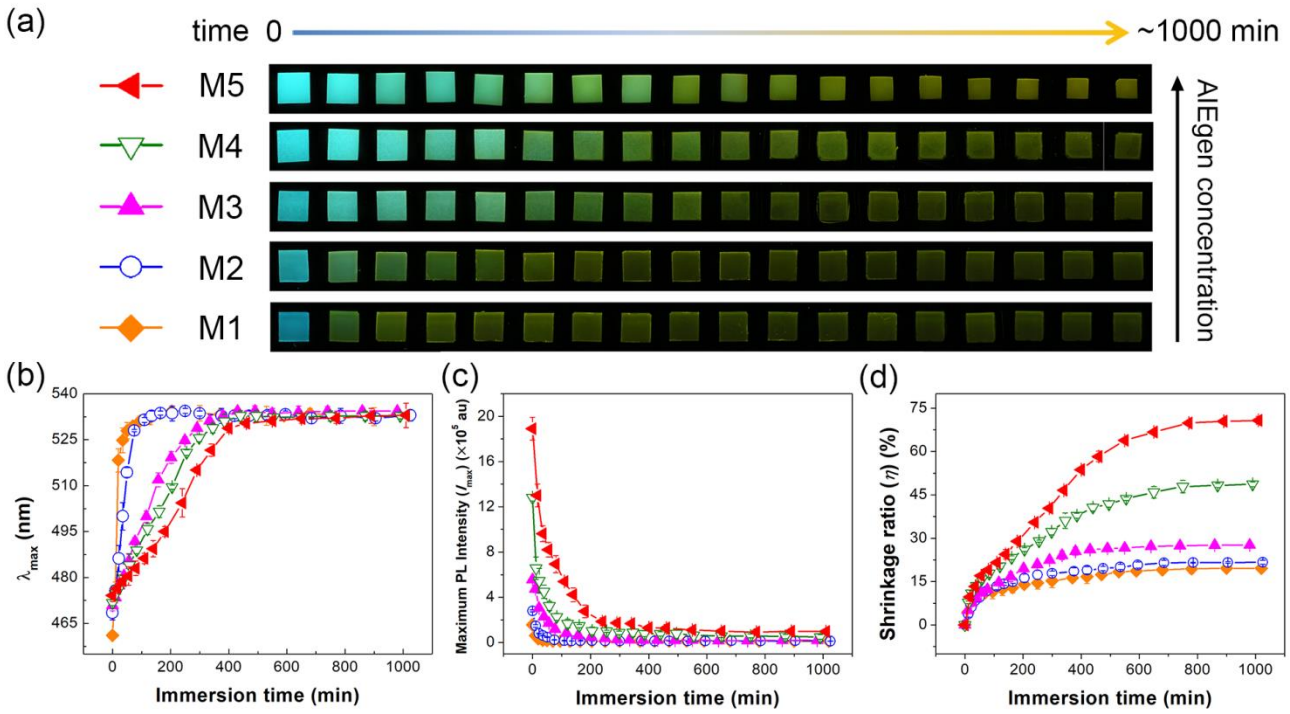

Figure 4. (a) Photographs of monolayer hydrogel samples **M1** to **M5** after immersed in pH 3.12 aqueous solution with different time under 365-nm UV illumination. (The immersion time of every hydrogel samples from left to right are about 0, 15, 35, 55, 80, 110, 140, 180, 240, 300, 350, 400, 450, 550, 650, 750, 900 and 1000 min respectively.) (b) λ_{max} of monolayer hydrogel samples as a function of immersion time after immersed in pH 3.12 aqueous solution. (c) I_{max} of monolayer hydrogel samples as a function of immersion time after immersed in pH 3.12 aqueous solution. (d) η of monolayer hydrogel samples as a function of immersion time after immersed in pH 3.12 aqueous solution.

sulfonate groups on PAAm-*r*-PSS leads to the shielding effect on 4H-TPE-4Py^{4+} protons, which causes their signal to upfield shift.[83] On the other hand, signals of protons H_a and H_b on the benzenesulfonate group on PAAm-*r*-PSS shift downfield in Figure 3e (IV) compared with that in Figure 3e (III). This is caused by the interaction with the protonated pridyl groups on 4H-TPE-4Py^{4+}. 2D NOESY ^{1}H NMR spectra of the D_2O solution containing both PAAm-*r*-PSS and TPE-4Py with the pH value of 2.0 was also taken. From the spectrum (Figure 3f) it can be seen that signals of protons on protonated pridyl groups in 4H-TPE-4Py^{4+} correlate with the resonance of benzenesulfonate protons on PAAm-*r*-PSS. The correlation peaks can not found in the spectrum of the D_2O solution of TPE-4Py with the pH value of 2.0 (Figure S4). The above NMR results all indicate that electrostatic interactions exist between 4H-TPE-4Py^{4+} and benzenesulfonate groups on the hydrogel network chains.

Dynamic Feature of pH-Responsive Fluorescence Color, Brightness and Volume Changing Properties of TPE-4Py/PAS-Based Monolayer Hydrogels. After the study of the pH-responsiveness of fluorescence color, brightness and volume of TPE-4Py/PAS-based monolayer hydrogels in different pH values, 3.12 was selected as the pH value to investigate the dynamic process of the fluorescence color, brightness and volume changing of the hydrogels. Swollen hydrogel sheets of **M1** to **M5** with the size of about 10 mm × 10 mm were immersed in aqueous solutions with the pH value of 3.12. Photographs under 365-nm UV illumination, fluorescent emission spectra (Figure S13) and masses of the hydrogel sheets at different time were measured. Time dependences of λ_{max} and I_{max} were depicted in Figure 4b and c. It can be seen from the photographs (Figure 4a) and the figures that for all hydrogels with the increase of the immersion time, the fluorescent emission red shifts and the fluorescent intensity decreases. These were caused by the protonation of TPE-4Py and the EIR effect of protonated TPE-4Py. With the increase of TPE-4Py concentration from **M1** to **M5**, the time which the hydrogels spend to reach the equilibrated λ_{max} values about 533 nm and the equilibrated I_{max} values increases. With the increase of the amount of TPE-4Py molecules in the hydrogel sheet, the time that the molecules spend to protonate to 4H-TPE-4Py^{4+} increases. Meanwhile, η of all hydrogel sheets increases with the increase of the immersion time, and the time which the hydrogel sheets spend to reach the equilibrated η values increases with the increase of TPE-4Py concentration from **M1** to **M5** in Figure 4d. With the increase of the immersion time, the amount of physical cross-linking points (protonated TPE-4Py) increases, and the hydrogel shrink gradually. With the increase of the amount of TPE-4Py molecules in the hydrogel sheet, the time that the molecules spend to protonate to 4H-TPE-4Py^{4+} and form electrostatic interactions with hydrogel network chains increases. Because changes of the fluorescent emission wavelength, the fluorescent intensity and the volume of the monolayer hydrogels root in one element, TPE-4Py,

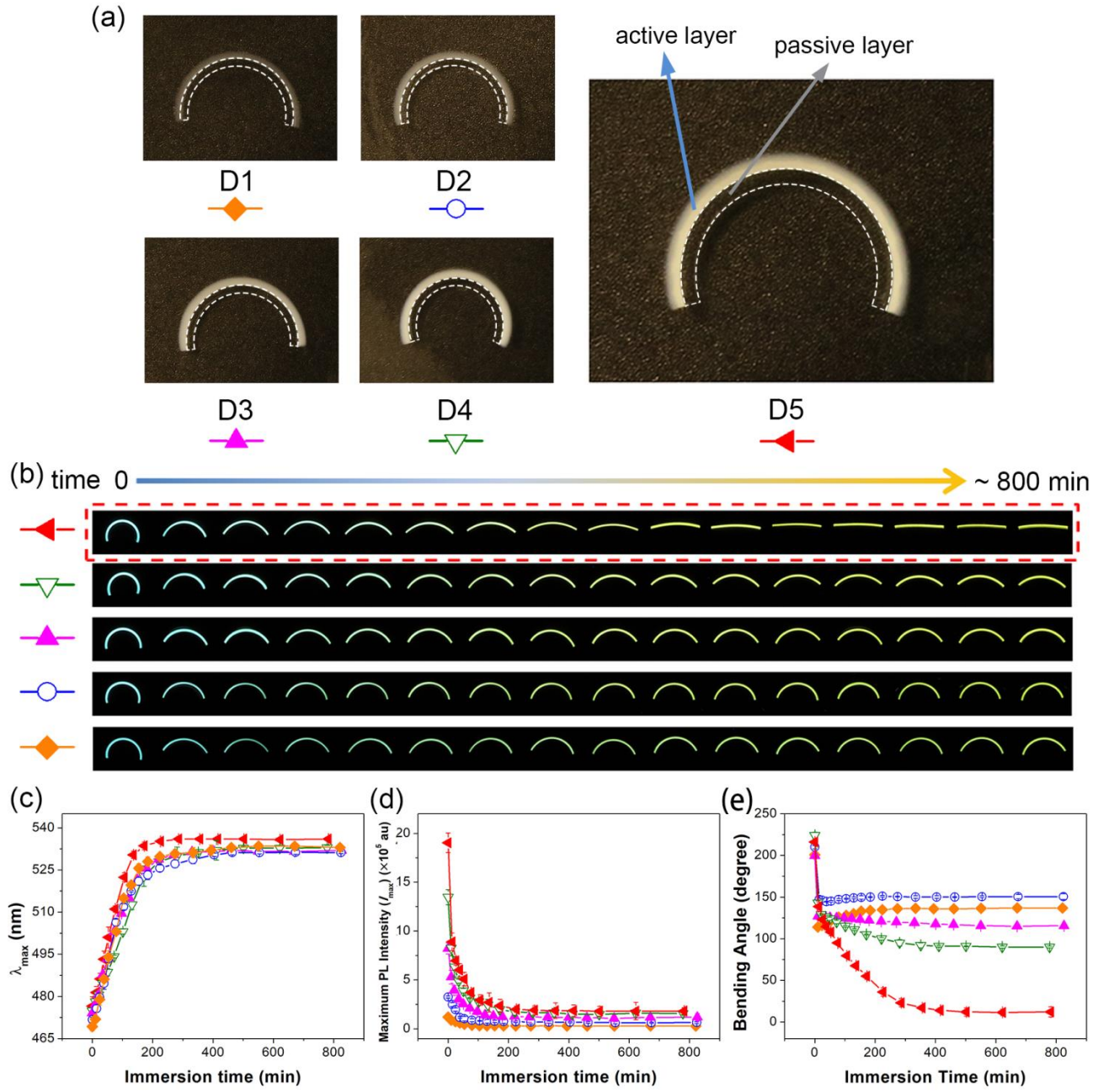

Figure 5. (a) Photographs of fully swollen bilayer hydrogel actuator samples **D1** to **D5** under day-light. (b) Photographs of the monolayer hydrogel samples after immersed in pH 3.12 aqueous solution with different time under 365-nm UV illumination. (The immersion time of every hydrogel samples from left to right are about 0, 12, 25, 38, 53, 77, 105, 135, 170, 225, 285, 355, 415, 500, 625, and 780 min.) (c) λ_{max} of the monolayer hydrogel samples as a function of immersion time after immersed in pH 3.12 aqueous solution. (d) I_{max} of the monolayer hydrogel samples as a function of immersion time after immersed in pH 3.12 aqueous solution. (e) Bending angle of the monolayer hydrogel samples as a function of immersion time after immersed in pH 3.12 aqueous solution.

the changes of the three properties are simultaneous and synchronous from Figure 4.

Dynamic pH-Responsive Fluorescence Color, Brightness Changing and Shape Deformation Properties of TPE-4Py/PAS-Based Bilayer Hydrogel Actuators. To transform the isotropic shrinkage of the monolayer hydrogels into anisotropic 3D shape deformation, bilayer hydrogel actuators were fabricated through a simple strategy of adding a PAS hydrogel layer without TPE-4Py (**Mo**) onto the TPE-4Py/PAS-based monolayer hydrogels (**M1** to **M5**). The TPE-4Py/PAS-based monolayer hydrogel acts as the role of the active layer and the PAS-based monolayer hydrogel acts as the role of the passive layer (Figure S5). Thus, two layers of the formed actuators are based on one hydrogel matrix of PAS with the difference that whether the function element TPE-4Py exists. Five bilayer hydrogel actuators **D1** to **D5** were prepared from **M1** to **M5** and **Mo** (Table S2) according to the procedure in the Supporting Information.

The as-prepared bilayer hydrogel actuators of **D1** to **D5** were cut into strips with the size of 15 mm × 2 mm, and were immersed in bulk DI water for 12 h. The equilibratedly swollen actuator strips are arc-shaped (Figure 5a) with the transparent passive layer at the inner layer and the white active layer at the outer layer. Auxiliary white dash lines were depicted in the photographs to facilitate the recognition of the passive layers.

The arc-shaped bilayer hydrogel actuator strips were immersed in aqueous solutions with the pH value of 3.12. Photographs under 365-nm UV illumination, fluorescent emission spectra (Figure S14) and bending angles of them at different time were measured. The fluorescent emission spectra were measured from the direction of the passive layer. Time dependences of λ_{max} and I_{max} were depicted in Figure 5c and d. It can be seen from the photographs (Figure 5b) and the figures that for all actuator strips with the increase of the immersion time, the fluorescent emission red shifts and the fluorescent intensity decreases. These were caused by the protonation of TPE-4Py and the EIR effect of protonated TPE-4Py in the active layer. With the increase of the TPE-4Py concentration in the active layer of the actuator strips from **D1** to **D5**, the time which the hydrogels spend to reach the equilibrated λ_{max} values and the equilibrated I_{max} values tends to be the same. This character is different from that of the monolayer hydrogels **M1** to **M5**. The fluorescent emission spectra were measured from the direction of the passive layer. Thus the spectra showed the fluorescent properties of TPE-4Py located at the interface between the active and the passive layers. The protonated TPE-4Py molecules could migrate into the passive layer in short distance and form electrostatic interactions with the network chains of the passive layer. These protonated TPE-4Py molecules mainly contribute to the fluorescent emission spectra of the bilayer hydrogel actuators. Under this circumstance, the migration of the protonated TPE-4Py molecules is the key factor to determine the dynamics of the changing of the fluorescent properties of the actuators. The migration rates of the protonated TPE-4Py are consistent in all bilayer hydrogels. Thus the dynamics of the fluorescent properties changing of **D1** to **D5** are similar. Meanwhile, after the arc-shaped bilayer hydrogel actuator strips were immersed in aqueous solutions with the pH value of 3.12, the strips gradually unbent (Figure 5b). Time dependences of bending angles of the strips were depicted in Figure 5e. It can be seen from the figure that with the increase of the immersion time, bending angles of all strips of **D1** to **D5** decrease gradually and finally reach equilibriums. With the increase of the immersion time, the increase of the amount of physical cross-linking points (protonated TPE-4Py) causes the active layer to shrink, and the generated force at the interface between the active and the passive layers causes the actuator strips to unbend. With the increase of the immersion time, bending angles of actuator strips **D1** and **D2** first quickly decrease, then increase a little, and finally reach equilibriums. After the actuator strips were immersed in the pH 3.12 aqueous solution, the TPE-4Py first protonated and formed electrostatic interactions with network chains of the active layer. These newly formed physical cross-linking points resulted in the shrinkage of the active layer and the unbending of the strips. Then a small amount of protonated TPE-4Py molecules migrated into the passive layer and acted as the physical cross-linking points to interact with its network chains. This caused the passive layer to shrink slightly, and the strips recovered slightly. When the TPE-4Py concentration in the active layer further increases, this bending angle recovery phenomenon disappears for **D3** to **D5**. The newly formed protonated TPE-4Py could either form interactions with network chains in the active layer or migrate and form interactions with network chains in the passive layer. Nevertheless, the amount of the migrated protonated TPE-4Py molecules is small and the majority of the protonated TPE-4Py molecules act as the physical cross-linking points in the active layer. When the TPE-4Py concentration increases in the active layer, the proportion of the amount of the migrated protonated TPE-4Py molecules in all protonated ones decreases, and the recovery effect can not be appeared. With the increase of the TPE-4Py concentration in the actuator strips from **D3** to **D5**, the time which the strips spend to reach equilibriums increases. With the increase of the amount of TPE-4Py molecules in the strips, the time that the molecules spend to protonate to 4H-TPE-4Py^{4+} and form electrostatic interactions with hydrogel network chains increases. From Figure 5b to e, it can be seen that the changes of the fluorescent emission wavelength, the fluorescent intensity and the bending angle of the bilayer hydrogel actuators are simultaneous and synchronous. This is profited from the core role of TPE-4Py as the origin of the changes of the three properties. Because the bilayer hydrogel actuator strip **D5** had the moderate changing rate of fluorescence color, brightness and curvature, it was selected to prepare the complex-shaped actuator and simulate the blooming process of natural flowers with the ability of simultaneous color changing during blooming.

A flower-shaped bilayer hydrogel actuator based on **D5** was prepared through cutting of the as-prepared **D5** bilayer hydrogel film. After the actuator was immersed in DI water to swell to the equilibrium, it turned into furling state. Then it was immersed in the aqueous solution with pH value of 3.12. Photographs of the actuator were taken every several minutes until 780 min from side and top views under 365-nm UV illumination. 18 photographs were selected to show the process of simultaneous fluorescence color and brightness changes and complex shape deformation of the actuator in Figure 6. It can be seen that with the increase of the immersion time, the artificial flower made by **D5** gradually blooms accompanied with simultaneous fluorescence color and brightness changes. All the photographs are also made into two movies (Movie M1 and M2).

AIE Effect during the Process of the Simultaneous Fluorescence Color, Brightness and Shape Changing of Bilayer Hydrogel Actuators. In the neutral medium, the origin of the fluorescence of the actuator is aggregated TPE-4Py encapsulated in the active layer.

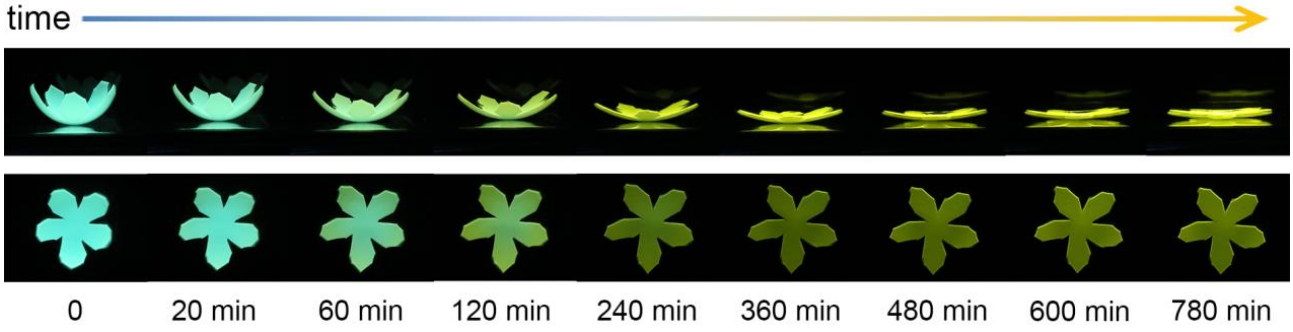

Figure 6. Simultaneous emission change and complex shape deformation of **M5** based hydrogel actuator. (Photographs were taken under 365-nm UV illumination. The upper line is flat view and the lower line is plane view.)

AIE effect causes the TPE-4Py to emit strong sapphire light. TPE-4Py forms aggregates in the neutral water and emits strong fluorescence. When TPE-4Py protonates to 4H-TPE-4Py^{4+} in the aqueous solution, the dissolution of 4H-TPE-4Py^{4+} activates its intromolecular rotation. Thus the red shifted fluorescent light of 4H-TPE-4Py^{4+} is pretty weak. The maximum PL intensity of the TPE-4Py suspension with the pH value of 6.98 ($I_{pH = 6.98}$) is 221.5 times that of the 4H-TPE-4Py^{4+} solution with the pH value of 3.34 ($I_{pH = 3.34}$) (Figure S16). Quantum yields (QYs) of the TPE-4Py suspensions with different pH values were also measured (Figure S15a), and QY of TPE-4Py suspension with the pH value of 6.98 ($QY_{pH = 6.98}$) is 8.6 times that of 4H-TPE-4Py^{4+} solution with the pH value of 3.34 ($QY_{pH = 3.34}$). However, for the TPE-4Py/PAS-based monolayer hydrogels and bilayer hydrogel actuators, the differences of fluorescence brightness before and after immersed in pH 3.12 aqueous solution are largely reduced. The maximum PL intensity of **D5** before the immersion ($I_{before\ immersion}$) is only 10.5 times that of it after the immersion ($I_{after\ immersion}$), and QY of **D5** before the immersion ($QY_{before\ immersion}$) is only 2.3 times that of it after the immersion ($QY_{after\ immersion}$). After the protonation of TPE-4Py, the formed 4H-TPE-4Py^{4+} electrostatically interacts with network chains of the hydrogel. These interactions and the network polymer chains largely restrict the intramolecular rotation of 4H-TPE-4Py^{4+}, which leads to the visible red shifted fluorescent emission.

CONCLUSIONS

In summary, bilayer hydrogel actuators with abilities of simultaneous fluorescence color and brightness changes and complex shape deformation under one stimulus were designed and fabricated using TPE-4Py as the core function element and PAS as the matrix. TPE-4Py aggregates encapsulated PAS hydrogel acted as the active layer of the actuators and blank PAS hydrogel acted as the passive layer. TPE-4Py/PAS-based monolayer hydrogels and bilayer hydrogel actuators with different TPE-4Py concentration were prepared and their pH-responsiveness was investigated. When the flower-shaped actuator **M5** were immersed in aqueous solution with pH value of 3.12, it could simultaneously change its fluorescence color, brightness and shape during 13 h. Protonation of TPE-4Py led to fluorescence color and brightness changes of the actuators and meanwhile electrostatic interactions occurred between the formed protonated TPE-4Py and benzenesulfonate groups on PAS chains in the active layer caused the actuators to deform. The strategy of combining AIEgens with bilayer hydrogels to construct stimuli-responsive hydrogels with complex practical functions in this work provides new insights in the design of intelligent systems. The prepared TPE-4Py/PAS-based bilayer hydrogel actuators are potential to be applied in high-tech fields such as 3D and 4D printing, soft robots, smart wearable devices and drug delivery systems.

ASSOCIATED CONTENT

Supporting Information.

Experimental Section and additional information related to the Results and Discussion section (PDF)

Movies M1 and M2

AUTHOR INFORMATION

Corresponding Author

*chjacky@ust.hk

*tangbenz@ust.hk

Notes

The authors declare no competing financial interest.

ACKNOWLEDGMENT

J. W. Y. L. and B.Z.T. acknowledge the financial support from the National Science Foundation of China (21788102, 21490570 and 21490574), the Research Grant Council of Hong Kong (16308116, 16305618 and C6009-17G), the Science and Technology Plan of Shenzhen (JCYJ20160229205601482, JCY20170307173739739 and JCYJ20170818113602462) and the Innovation and Technology Commission (ITC-CNERC149C01).

REFERENCES

(1) Schull, J. Are Species Intelligent? *Behav. Brain Sci.* **1990**, *13* (1), 63-75.

(2) van Loon, L. C. The Intelligent Behavior of Plants. *Trends Plant Sci.* **2016**, *21* (4), 286-294.

(3) Teyssier, J.; Saenko, S. V.; van der Marel, D.; Milinkovitch, M. C. Photonic crystals cause active colour change in chameleons. *Nat. Commun.* **2015**, *6*, 6368.

(4) Crookes, W. J.; Ding, L.-L.; Huang, Q. L.; Kimbell, J. R.; Horwitz, J.; McFall-Ngai, M. J. Reflectins: The Unusual Proteins of Squid Reflective Tissues. *Science* **2004**, *303* (5655), 235-238.

(5) Wilker, J. J. How to suck like an octopus. *Nature* **2017**, *546*, 358-359.

(6) Shine, R. Function and evolution of the frill of the frillneck lizard, Chlamydosaurus kingii (Sauria: Agamidae). *Biol. J. Linn. Soc.* **2008**, *40* (1), 11-20.

(7) Hamilton, D. G.; Whiting, M. J.; Pryke, S. R. Fiery frills: carotenoid-based coloration predicts contest success in frillneck lizards. *Behav. Ecol.* **2013**, *24* (5), 1138-1149.

(8) Vaknin, H.; Bar-Akiva, A.; Ovadia, R.; Nissim-Levi, A.; Forer, I.; Weiss, D.; Oren-Shamir, M. Active anthocyanin degradation in Brunfelsia calycina (yesterday-today-tomorrow) flowers. *Planta* **2005**, *222* (1), 19-26.

(9) Li, M.; Sun, Y. T.; Lu, X. C.; Debnath, B.; Mitra, S.; Qiu, D. L. Proteomics Reveal the Profiles of Color Change in Brunfelsia acuminata Flowers. *Int. J. Mol. Sci.* **2019**, *20* (8), 2000-2016.

(10) Eisikowitch, D.; Rotem, R. Flower Orientation and Color Change in Quisqualis Indica and Their Possible Role in Pollinator Partitioning. *Bot. Gaz.* **1987**, *148* (2), 175-179.

(11) Yan, J.; Wang, M.; Zhang, L. Light induces petal color change in Quisqualis indica (Combretaceae). *Plant Diversity* **2018**, *40* (1), 28-34.

(12) Pereira, A. C.; da Silva, J. B.; Goldenberg, R.; Melo, G. A. R.; Varassin, I. G. Flower color change accelerated by bee pollination in Tibouchina (Melastomataceae). *Flora* **2011**, *206* (5), 491-497.

(13) Weiss, M. R. Floral Color Changes as Cues for Pollinators. *Nature* **1991**, *354* (6350), 227-229.

(14) Wang, H.; Ji, X. F.; Li, Z. T.; Huang, F. H. Fluorescent Supramolecular Polymeric Materials. *Adv. Mater.* **2017**, *29* (14), 1606117.

(15) Zhang, X.; Chen, L. F.; Lim, K. H.; Gonuguntla, S.; Lim, K. W.; Pranantyo, D.; Yong, W. P.; Yam, W. J. T.; Low, Z.; Teo, W. J.; Nien, H. P.; Loh, Q. W.; Soh, S. The Pathway to Intelligence: Using Stimuli-Responsive Materials as Building Blocks for Constructing Smart and Functional Systems. *Adv. Mater.* **2019**, *31* (11), 1804540.

(16) Cobo, I.; Li, M.; Sumerlin, B. S.; Perrier, S. Smart hybrid materials by conjugation of responsive polymers to biomacromolecules. *Nat. Mater.* **2015**, *14* (2), 143-159.

(17) Yu, X. W.; Cheng, H. H.; Zhang, M.; Zhao, Y.; Qu, L. T.; Shi, G. Q. Graphene-based smart materials. *Nat. Rev. Mater.* **2017**, *2* (9), 17046.

(18) Xu, W. N.; Kwok, K. S.; Gracias, D. H. Ultrathin Shape Change Smart Materials. *Accounts Chem. Res.* **2018**, *51* (2), 436-444.

(19) Doring, A.; Birnbaum, W.; Kuckling, D. Responsive hydrogels - structurally and dimensionally optimized smart frameworks for applications in catalysis, micro-system technology and material science. *Chem. Soc. Rev.* **2013**, *42* (17), 7391-7420.

(20) Ji, X. F.; Huang, F. H. A rapidly self-healing supramolecular polymer hydrogel. *Sci. China-Chem.* **2015**, *58* (3), 436-437.

(21) Ma, C.; Le, X.; Tang, X.; He, J.; Xiao, P.; Zheng, J.; Xiao, H.; Lu, W.; Zhang, J.; Huang, Y.; Chen, T. A Multiresponsive Anisotropic Hydrogel with Macroscopic 3D Complex Deformations. *Adv. Funct. Mater.* **2016**, *26* (47), 8670-8676.

(22) Wei, S.; Lu, W.; Le, X.; Ma, C.; Lin, H.; Wu, B.; Zhang, J.; Theato, P.; Chen, T. Bioinspired Synergistic Fluorescence-Color Switchable Polymeric Hydrogel Actuator. *Angew. Chem., Int. Edit.* **2019**. DOI: 10.1002/anie.201908437.

(23) Ilmain, F.; Tanaka, T.; Kokufuta, E. Volume transition in a gel driven by hydrogen bonding. *Nature* **1991**, *349* (6308), 400-401.

(24) Xia, L. W.; Xie, R.; Ju, X. J.; Wang, W.; Chen, Q. M.; Chu, L. Y. Nano-structured smart hydrogels with rapid response and high elasticity. *Nat. Commun.* **2013**, *4*, 2226.

(25) Zhang, X. N.; Wang, Y. J.; Sun, S.; Hou, L.; Wu, P.; Wu, Z. L.; Zheng, Q. A Tough and Stiff Hydrogel with Tunable Water Content and Mechanical Properties Based on the Synergistic Effect of Hydrogen Bonding and Hydrophobic Interaction. *Macromolecules* **2018**, *51* (20), 8136-8146.

(26) Lee, K.; Asher, S. A. Photonic Crystal Chemical Sensors: pH and Ionic Strength. *J. Am. Chem. Soc.* **2000**, *122* (39), 9534-9537.

(27) Ma, C.; Li, T.; Zhao, Q.; Yang, X.; Wu, J.; Luo, Y.; Xie, T. Supramolecular Lego Assembly Towards Three-Dimensional Multi-Responsive Hydrogels. *Adv. Mater.* **2014**, *26* (32), 5665-5669.

(28) Mamada, A.; Tanaka, T.; Kungwatchakun, D.; Irie, M. Photoinduced phase transition of gels. *Macromolecules* **1990**, *23* (5), 1517-1519.

(29) Wang, H.; Zhu, C. N.; Zeng, H.; Ji, X. F.; Xie, T.; Yan, X. Z.; Wu, Z. L.; Huang, F. H. Reversible Ion-Conducting Switch in a Novel Single-Ion Supramolecular Hydrogel Enabled by Photoresponsive Host-Guest Molecular Recognition. *Adv. Mater.* **2019**, *31* (12), 1807328.

(30) Tanaka, T.; Nishio, I.; Sun, S. T.; Uenonishio, S. Collapes of Gels in An Electric-Field. *Science* **1982**, *218* (4571), 467-469.

(31) Hu, K.; Sun, J.; Guo, Z.; Wang, P.; Chen, Q.; Ma, M.; Gu, N. A Novel Magnetic Hydrogel with Aligned Magnetic Colloidal Assemblies Showing Controllable Enhancement of Magnetothermal Effect in the Presence of Alternating Magnetic Field. *Adv. Mater.* **2015**, *27* (15), 2507-2514.

(32) Zheng, S. Y.; Shen, Y.; Zhu, F.; Yin, J.; Qian, J.; Fu, J.; Wu, Z. L.; Zheng, Q. Programmed Deformations of 3D-Printed Tough Physical Hydrogels with High Response Speed and Large Output Force. *Adv. Funct. Mater.* **2018**, *28* (37), 1803366.

(33) Tu, T.; Fang, W.; Sun, Z. Visual-Size Molecular Recognition Based on Gels. *Adv. Mater.* **2013**, *25* (37), 5304-5313.

(34) Jia, H.; Li, Z.; Wang, X.; Zheng, Z. Facile functionalization of a tetrahedron-like PEG macromonomer-based fluorescent hydrogel with high strength and its heavy metal ion detection. *J. Mater. Chem. A* **2015**, *3* (3), 1158-1163.

(35) Stoychev, G.; Zakharchenko, S.; Turcaud, S.; Dunlop, J. W. C.; Ionov, L. Shape-Programmed Folding of Stimuli-Responsive Polymer Bilayers. *ACS Nano* **2012**, *6* (5), 3925-3934.

(36) Yao, C.; Liu, Z.; Yang, C.; Wang, W.; Ju, X. J.; Xie, R.; Chu, L. Y. Poly(N-isopropylacrylamide)-Clay Nanocomposite Hydrogels with Responsive Bending Property as Temperature-Controlled Manipulators. *Adv. Funct. Mater.* **2015**, *25* (20), 2980-2991.

(37) Stoychev, G.; Guiducci, L.; Turcaud, S.; Dunlop, J. W. C.; Ionov, L. Hole-Programmed Superfast Multistep Folding of Hydrogel Bilayers. *Adv. Funct. Mater.* **2016**, *26* (42), 7733-7739.

(38) Liu, L.; Ghaemi, A.; Gekle, S.; Agarwal, S. One-Component Dual Actuation: Poly(NIPAM) Can Actuate to Stable 3D Forms with Reversible Size Change. *Adv. Mater.* **2016**, *28* (44), 9792-9796.

(39) Kim, D.; Kim, H.; Lee, E.; Jin, K. S.; Yoon, J. Programmable Volume Phase Transition of Hydrogels Achieved by Large Thermal Hysteresis for Static-Motion Bilayer Actuators. *Chem. Mater.* **2016**, *28* (23), 8807-8814.

(40) Duan, J.; Liang, X.; Zhu, K.; Guo, J.; Zhang, L. Bilayer hydrogel actuators with tight interfacial adhesion fully constructed from natural polysaccharides. *Soft Matter* **2017**, *13* (2), 345-354.

(41) Wang, Z. J.; Hong, W.; Wu, Z. L.; Zheng, Q. Site-Specific Pre-Swelling-Directed Morphing Structures of Patterned Hydrogels. *Angew. Chem., Int. Ed.* **2017**, *56* (50), 15974-15978.

(42) Cheng, Y.; Huang, C.; Yang, D.; Ren, K.; Wei, J. Bilayer hydrogel mixed composites that respond to multiple stimuli for environmental sensing and underwater actuation. *J. Mater. Chem. B* **2018**, *6* (48), 8170-8179.

(43) Gao, G.; Wang, Z.; Xu, D.; Wang, L.; Xu, T.; Zhang, H.; Chen, J.; Fu, J. Snap-Buckling Motivated Controllable Jumping of Thermo-Responsive Hydrogel Bilayers. *ACS Appl. Mater. Interfaces* **2018**, *10* (48), 41724-41731.

(44) Hu, Z.; Zhang, X.; Li, Y. Synthesis and application of modulated polymer gels. *Science* **1995**, *269* (5223), 525-527.

(45) Haque, M. A.; Kamita, G.; Kurokawa, T.; Tsujii, K.; Gong, J. P. Unidirectional Alignment of Lamellar Bilayer in Hydrogel: One-Dimensional Swelling, Anisotropic Modulus, and Stress/Strain Tunable Structural Color. *Adv. Mater.* **2010**, *22* (45), 5110-5114.

(46) Zhang, Q. M.; Xu, W.; Serpe, M. J. Optical Devices Constructed from Multiresponsive Microgels. *Angew. Chem., Int. Ed.* **2014**, *53* (19), 4827-4831.

(47) Görl, D.; Soberats, B.; Herbst, S.; Stepanenko, V.; Würthner, F. Perylene bisimide hydrogels and lyotropic liquid crystals with temperature-responsive color change. *Chem. Sci.* **2016**, *7* (11), 6786-6790.

(48) Lu, W.; Ma, C.; Zhang, D.; Le, X.; Zhang, J.; Huang, Y.; Huang, C.-F.; Chen, T. Real-Time in Situ Investigation of Supramolecular Shape Memory Process by Fluorescence Switching. *J. Phys. Chem. C* **2018**, *122* (17), 9499-9506.

(49) Mei, J.; Leung, N. L. C.; Kwok, R. T. K.; Lam, J. W. Y.; Tang, B. Z. Aggregation-Induced Emission: Together We Shine, United We Soar! *Chem. Rev.* **2015**, *115* (21), 11718-11940.

(50) Luo, J. D.; Xie, Z. L.; Lam, J. W. Y.; Cheng, L.; Chen, H. Y.; Qiu, C. F.; Kwok, H. S.; Zhan, X. W.; Liu, Y. Q.; Zhu, D. B.; Tang, B. Z. Aggregation-induced emission of 1-methyl-1,2,3,4,5-pentaphenylsilole. *Chem. Commun.* **2001**(18), 1740-1741.

(51) Mei, J.; Hong, Y.; Lam, J. W. Y.; Qin, A.; Tang, Y.; Tang, B. Z. Aggregation-Induced Emission: The Whole Is More Brilliant than the Parts. *Adv. Mater.* **2014**, *26* (31), 5429-5479.

(52) Zheng, H. Y.; Li, C. Y.; He, C. C.; Dong, Y. Q.; Liu, Q. S.; Qin, P. F.; Zeng, C.; Wang, H. L. Luminescent hydrogels based on di(4-propoxyphenyl)-dibenzofulvene exhibiting four emission colours and organic solvents/thermal dual-responsive properties. *J. Mater. Chem. C* **2014**, *2* (29), 5829-5835.

(53) Wang, Z. K.; Nie, J. Y.; Qin, W.; Hu, Q. L.; Tang, B. Z. Gelation process visualized by aggregation-induced emission fluorogens. *Nat. Commun.* **2016**, *7*, 12033.

(54) Yan, X. Z.; Cook, T. R.; Wang, P.; Huang, F. H.; Stang, P. J. Highly emissive platinum(II) metallacages. *Nat. Chem.* **2015**, *7* (4), 342-348.

(55) Hu, R. R.; Kang, Y.; Tang, B. Z. Recent advances in AIE polymers. *Polym. J.* **2016**, *48* (4), 359-370.

(56) Feng, H. T.; Yuan, Y. X.; Xiong, J. B.; Zheng, Y. S.; Tang, B. Z. Macrocycles and cages based on tetraphenylethylene with aggregation-induced emission effect. *Chem. Soc. Rev.* **2018**, *47* (19), 7452-7476.

(57) Qi, J.; Chen, C.; Ding, D.; Tang, B. Z. Aggregation-Induced Emission Luminogens: Union Is Strength, Gathering Illuminates Healthcare. *Adv. Healthcare Mater.* **2018**, *7* (20), 1800477.

(58) Ji, X.; Shi, B.; Wang, H.; Xia, D.; Jie, K.; Wu, Z. L.; Huang, F. Supramolecular Construction of Multifluorescent Gels: Interfacial Assembly of Discrete Fluorescent Gels through Multiple Hydrogen Bonding. *Adv. Mater.* **2015**, *27* (48), 8062-8066.

(59) Dong, Y. Q.; Lam, J. W. Y.; Qin, A.; Sun, J. X.; Liu, J. Z.; Li, Z.; Sun, J. Z.; Sung, H. H. Y.; Williams, I. D.; Kwok, H. S.; Tang, B. Z. Aggregation-induced and crystallization-enhanced emissions of 1,2-diphenyl-3,4-bis(diphenylmethylene)-1-cyclobutene. *Chem. Commun.* **2007**(31), 3255-3257.

(60) Lin, Q.; Lu, T.-T.; Zhu, X.; Wei, T.-B.; Li, H.; Zhang, Y.-M. Rationally introduce multi-competitive binding interactions in supramolecular gels: a simple and efficient approach to develop multi-analyte sensor array. *Chem. Sci.* **2016**, *7* (8), 5341-5346.

(61) Cheng, Y.; Wang, J.; Qiu, Z.; Zheng, X.; Leung, N. L. C.; Lam, J. W. Y.; Tang, B. Z. Multiscale Humidity Visualization by Environmentally Sensitive Fluorescent Molecular Rotors. *Adv. Mater.* **2017**, *29* (46), 1703900.

(62) Liu, S.; Cheng, Y.; Zhang, H.; Qiu, Z.; Kwok, R. T. K.; Lam, J. W. Y.; Tang, B. Z. In Situ Monitoring of RAFT Polymerization by Tetraphenylethylene-Containing Agents with Aggregation-Induced Emission Characteristics. *Angew. Chem., Int. Ed.* **2018**, *57* (21), 6274-6278.

(63) Cheng, Y. H.; Liu, S. J.; Song, F. Y.; Khorloo, M.; Zhang, H. K.; Kwok, R. T. K.; Lam, J. W. Y.; He, Z. K.; Tang, B. Z. Facile emission color tuning and circularly polarized light generation of single luminogen in engineering robust forms. *Mater. Horizons* **2019**, *6* (2), 405-411.

(64) Mutai, T.; Tomoda, H.; Ohkawa, T.; Yabe, Y.; Araki, K. Switching of Polymorph-Dependent ESIPT Luminescence of an Imidazo[1,2-a]pyridine Derivative. *Angew. Chem., Int. Ed.* **2008**, *47* (49), 9522-9524.

(65) Chen, X.; Shen, X. Y.; Guan, E.; Liu, Y.; Qin, A.; Sun, J. Z.; Tang, B. Z. A pyridinyl-functionalized tetraphenylethylene fluorogen for specific sensing of trivalent cations. *Chem. Commun.* **2013**, *49* (15), 1503-1505.

(66) Furukawa, S.; Shono, H.; Mutai, T.; Araki, K. Colorless, Transparent, Dye-Doped Polymer Films Exhibiting Tunable Luminescence Color: Controlling the Dual-Color Luminescence of 2-(2′-Hydroxyphenyl)imidazo[1,2-a]pyridine Derivatives with the Surrounding Matrix. *ACS Appl. Mater. Interfaces* **2014**, *6* (18), 16065-16070.

(67) Wang, J. G.; Gu, X. G.; Zhang, P. F.; Huang, X. B.; Zheng, X. Y.; Chen, M.; Feng, H. T.; Kwok, R. T. K.; Lam, J. W. Y.; Tang, B. Z. Ionization and Anion-pi(+) Interaction: A New Strategy for Structural Design of Aggregation-Induced Emission Luminogens. *J. Am. Chem. Soc.* **2017**, *139* (46), 16974-16979.

(68) Feng, X.; Li, Y.; He, X.; Liu, H.; Zhao, Z.; Kwok, R. T. K.; Elsegood, M. R. J.; Lam, J. W. Y.; Tang, B. Z. A Substitution-Dependent Light-Up Fluorescence Probe for Selectively Detecting Fe3+ Ions and Its Cell Imaging Application. *Adv. Funct. Mater.* **2018**, *28* (35), 1802833.

(69) Sun, Y.; Yao, Y.; Wang, H.; Fu, W.; Chen, C.; Saha, M. L.; Zhang, M.; Datta, S.; Zhou, Z.; Yu, H.; Li, X.; Stang, P. J. Self-Assembly of Metallacages into Multidimensional Suprastructures with Tunable Emissions. *J. Am. Chem. Soc.* **2018**, *140* (40), 12819-12828.

(70) Yan, X.; Wang, F.; Zheng, B.; Huang, F. Stimuli-responsive supramolecular polymeric materials. *Chem. Soc. Rev.* **2012**, *41* (18), 6042-6065.

(71) Wei, P.; Yan, X.; Huang, F. Supramolecular polymers constructed by orthogonal self-assembly based on host–guest and metal–ligand interactions. *Chem. Soc. Rev.* **2015**, *44* (3), 815-832.

(72) Wang, M.; Zheng, Y. R.; Ghosh, K.; Stang, P. J. Metallosupramolecular Tetragonal Prisms via Multicomponent Coordination-Driven Template-Free Self-Assembly. *J. Am. Chem. Soc.* **2010**, *132* (18), 6282-6283.

(73) Sun, Y.; Zhang, F.; Jiang, S.; Wang, Z.; Ni, R.; Wang, H.; Zhou, W.; Li, X.; Stang, P. J. Assembly of Metallacages into Soft Suprastructures with Dimensions of up to Micrometers and the Formation of Composite Materials. *J. Am. Chem. Soc.* **2018**, *140* (49), 17297-17307.

(74) Ji, X.; Li, Z.; Liu, X.; Peng, H.-Q.; Song, F.; Qi, J.; Lam, J. W. Y.; Long, L.; Sessler, J. L.; Tang, B. Z. A Functioning Macroscopic "Rubik's Cube" Assembled via Controllable Dynamic Covalent Interactions. *Adv. Mater.* **2019**, 1902365. DOI : 10.1002/adma.201902365.

(75) Shi, J.; Chang, N.; Li, C.; Mei, J.; Deng, C.; Luo, X.; Liu, Z.; Bo, Z.; Dong, Y. Q.; Tang, B. Z. Locking the phenyl rings of tetraphenylethene step by step: understanding the mechanism of aggregation-induced emission. *Chem. Commun.* **2012**, *48* (86), 10675-10677.

(76) Zhang, G.-F.; Chen, Z.-Q.; Aldred, M. P.; Hu, Z.; Chen, T.; Huang, Z.; Meng, X.; Zhu, M.-Q. Direct validation of the restriction of intramolecular rotation hypothesis via the synthesis of novel ortho-methyl substituted tetraphenylethenes and their application in cell imaging. *Chem. Commun.* **2014**, *50* (81), 12058-12060.

(77) Lu, H. G.; Zheng, Y. D.; Zhao, X. W.; Wang, L. J.; Ma, S. Q.; Han, X. Q.; Xu, B.; Tian, W. J.; Gao, H. Highly Efficient Far Red/Near-Infrared Solid Fluorophores: Aggregation-Induced Emission, Intramolecular Charge Transfer, Twisted Molecular Conformation, and Bioimaging Applications. *Angew. Chem., Int. Edit.* **2016**, *55* (1), 155-159.

(78) Huang, Y. H.; Mei, J.; Ma, X. A novel simple red emitter characterized with AIE plus intramolecular charge transfer effects and its application for thiol-containing amino acids detection. *Dyes Pigment.* **2019**, *165*, 499-507.

(79) Wang, H.; Ji, X.; Li, Y.; Li, Z.; Tang, G.; Huang, F. An ATP/ATPase responsive supramolecular fluorescent hydrogel constructed via electrostatic interactions between poly(sodium *p*-styrenesulfonate) and a tetraphenylethene derivative. *J. Mater. Chem. B* **2018**, *6* (18), 2728-2733.

(80) Sun, H. W.; Zhang, Y.; Yan, W.; Chen, W. X.; Lan, Q.; Liu, S. W.; Jiang, L.; Chi, Z. G.; Chen, X. D.; Xu, J. R. A novel ultrasound-sensitive mechanofluorochromic AIE-compound with remarkable blue-shifting and enhanced emission. *J. Mater. Chem. C* **2014**, *2* (29), 5812-5817.

(81) Fateminia, S. M. A.; Wang, Z. M.; Goh, C. C.; Manghnani, P. N.; Wu, W. B.; Mao, D.; Ng, L. G.; Zhao, Z. J.; Tang, B. Z.; Liu, B. Nanocrystallization: A Unique Approach to Yield Bright Organic Nanocrystals for Biological Applications. *Adv. Mater.* **2017**, *29* (1), 1604100.

(82) Li, Z.; Zheng, Z.; Su, S.; Yu, L.; Wang, X. L. Preparation of a High-Strength Hydrogel with Slidable and Tunable Potential Functionalization Sites. *Macromolecules* **2016**, *49* (1), 373-386.

(83) Li, Z.; Zheng, Z.; Su, S.; Yu, L.; Wang, X. Hydroxypropyl-β-CD vs. Its α-Homologue for a 3D Modified Polyrotaxane Network Formation and Properties: the Relationship between Modified CD and Polymer Revealed through Comparison. *Soft Matter* **2016**, *12* (34), 7089-7101.

For Table of Contents Only

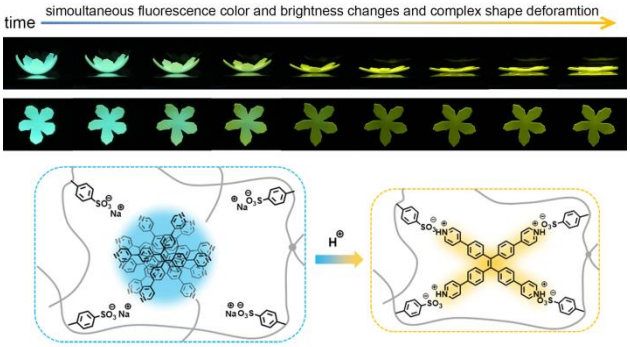
time
simoultaneous fluorescence color and brightness changes and complex shape deforamtion
H